Comptes Rendus

Mécanique

Nicolas Carrère, Aurélien Doitrand, Mathilde Conan and Eric Martin

Mechanisms of transverse cracking induced by adjacent ply matrix cracks in composite laminates

Research article / *Article de recherche*

Mechanisms of transverse cracking induced by adjacent ply matrix cracks in composite laminates

Mécanismes de fissuration transverse induits par des fissures matricielles dans des plis adjacents de stratifiés composites

Nicolas Carrère [ID],[a], **Aurélien Doitrand** [*],[ID],[b], **Mathilde Conan** [a] and **Eric Martin** [c]

[a] ENSTA Bretagne, CNRS, IRDL, UMR 6027, F-29806 Brest, France

[b] Université Lyon, INSA-Lyon, UCBL, CNRS, MATEIS, UMR5510, F-69621 Villeurbanne, France

[c] Bordeaux-INP, Univ. Bordeaux, F-33400 Talence, France

E-mails: nicolas.carrere@ensta-bretagne.fr (N. Carrère),
aurelien.doitrand@insa-lyon.fr (A. Doitrand), mathilde.conan@ensta-bretagne.org
(M. Conan), eric.martin@enseirb-matmeca.fr (E. Martin)

Abstract. Cracking in composite laminates containing θ-plies adjacent to 90° plies is studied experimentally and numerically using the coupled criterion and finite element calculations. Different damage mechanisms are considered, namely transverse cracking in 90°, cracking in θ-plies, or debonding between adjacent misoriented plies. The influence of the stacking sequence on the damage mechanism sequence is investigated. Experimental observations of the composite edge under tensile loading evidence θ-ply cracking (i) at an imposed strain level much larger than first transverse cracking in 90° ply for a sufficiently large orientation mismatch between adjacent plies or (ii) at a similar imposed strain level if the mismatch angle between two adjacent plies is small. The latter phenomenon may be mitigated by the presence of a 0° ply between the 90° and the θ-plies.

These conclusions are supported by numerical simulation of the experimentally observed damage mechanisms, evidencing a change in the damage mechanism sequence depending on the θ-ply misorientation. The numerical simulations also highlight that debonding between adjacent plies may occur as it becomes more favorable that adjacent ply crack re-initiation for sufficiently large adjacent ply mismatch angle.

Résumé. La fissuration dans les stratifiés composites, contenant des plis orientés à θ° de la direction de chargement adjacents à des plis à 90°, est étudiée expérimentalement et numériquement à l'aide du critère couplé et de calculs par éléments finis. Différents mécanismes d'endommagement sont pris en compte : la fissuration transverse dans le pli à 90°, la fissuration dans les plis à θ°, ou la décohésion entre des plis adjacents d'orientation différente. L'influence de la séquence d'empilement sur la séquence des mécanismes d'endommagement est analysée. Les observations expérimentales effectuées sur des stratifiés sollicités en traction mettent en évidence une fissuration dans les plis à θ : (i) à un niveau de déformation imposé beaucoup plus élevé que celui de la première fissuration transverse dans les plis à 90° pour une désorientation suffisamment grand entre les plis adjacents, ou (ii) à un niveau de déformation imposé similaire si l'angle de

---

[*] Corresponding author

désorientation entre deux plis adjacents est faible. Ce dernier phénomène peut être atténué par la présence d'un pli à 0° entre le pli à 90° et les plis à θ.

Ces conclusions sont appuyées par des simulations numériques des mécanismes d'endommagement observés expérimentalement, mettant en évidence un changement dans la séquence des mécanismes en fonction de l'angle de désorientation des plis à θ. Les simulations numériques montrent également que la décohésion entre plis adjacents peut se produire et devenir plus favorable que le ré-amorçage des fissures dans les plis adjacents lorsque l'angle de désorientation entre ces plis est suffisamment grand.

1. Introduction

The growing utilization of composite materials in sectors demanding both performance and safety is often guided by principles derived from lessons learned. In specific industries, such as aeronautics, these principles have been formalized into comprehensive best practice guidelines outlined in the Military Handbook [1]. This document outlines, among other aspects, the draping recommendations that must be complied with when defining the lay-up of a laminated composite structure. Among the draping recommendations details, we can mention for example:

(1) Homogeneous stacking sequence are recommended for strength controlled designs. The handbook reminds that *the interlaminar stress distributions are affected, around the periphery of holes, by the variation of ply orientations relative to a tangent to the edge. Since it is difficult to optimize for a single lay-up in this case, the best solution is to make the stacking sequence as homogeneous as possible.*

(2) Since transverse strength is highly dependent on ply thickness, it is strongly recommended to *minimize the grouping of plies with identical orientations,*

(3) The mismatch in Poisson's ratio between adjacent plies, caused by the anisotropy of the ply properties and the difference in orientation between them, can generate out-of-plane stresses at the interface of adjacent plies near the edges of a laminate. It is thus recommended to perform analyses *to predict free edge stresses and delamination strain levels.*

(4) It is recommended that the laminate has at least four distinct ply angles (e.g., 0°, $\pm\theta°$, 90°) with a minimum of 10% of the plies oriented at each angle.

These recommendations are partly based on experimental observations. Among numerous examples, and without claiming to be exhaustive, we can highlight a few studies that illustrate the aforementioned recommendations. Regarding recommendation #2, the pioneering work published in [2] demonstrated that thickness has a significant influence on the apparent strength of the ply. The impact of blocked versus dispersed plies on strength (recommendation #1) has been illustrated, for example, in unnotched specimens [3] and in open-hole specimens [4]. Delamination initiated from the edge and the effect of the stacking sequence (recommendation #3) have been studied in [5]. Finally, regarding the recommendation #4, the use of 0°, ±45°, 90° plies is a well-established practice driven by the need to balance stiffness, strength, processability, and damage tolerance. These orientations offer a versatile and practical solution for a wide range of engineering applications. It is essential to remember that the recommendations provided in this handbook serve solely as guidelines that should be verified based on the materials used and further assessed in relation to new-generation materials and manufacturing processes. Considering the high cost of testing and the numerous optimization possibilities [6], using models to estimate the influence of stacking on the laminate's strength is crucial.

Various models with differing levels of complexity have been proposed in the literature to achieve this goal. Classical Laminate Theory (CLT) is a simple and widely used model for rapidly designing laminated composite structures [7, 8]. Based on the elastic properties of the individual laminae, the stacking sequence, and the applied loading, this model enables the determination of the laminate's overall elastic properties and the stress distribution within each ply, while accounting for the effects of potential ply failure [9]. However, due to its inherent assumptions, this theory cannot account for the effects of discrete ply failure on adjacent plies or the potential delamination between two plies, whether caused by edge effects or induced by transverse failure. To effectively describe some of these mechanisms, it is essential to capture the discrete nature of the damage, such as transverse crack and delamination [10], particularly in terms of how a ply failure affects the neighboring plies [11, 12]. This approach holds significant potential for accurately describing the phenomena observed experimentally; however, it relies on sophisticated finite element models combined with highly non-linear material behaviors. Consequently, this often results in high computational costs, limiting the applicability of these methods for parametric studies or optimization.

The coupled criterion (CC), introduced by Leguillon in [13, 14], provides an efficient approach to address this challenge while preserving a discrete representation of the damage. It requires only a few elastic calculations to compute the stress field in the plane of the potential crack and the energy released by the crack initiation. It has been applied on composite materials in order to study several of the aforementioned issues [15]. The CC was used to study crack initiation in open hole composite plates [16–19] or in fastened joints composites [20] (recommendation #1 underlined at the beginning of this introduction and taken from the Military Handbook). Regarding composite laminates, the focus was mainly made on transverse cracking in 90° plies (i.e. when the loading direction is perpendicular to the fiber direction) and the effect of the number of grouped plies on the apparent strength (recommandation #2). This topic was studied in 2D [14, 21–23] or 3D [24, 25], also considering manufacturing thermal residual stresses [26, 27]. The CC has also been employed to investigate the onset of free-edge delamination in angle-ply laminates [28] (recommendation #3). Additionally, it has been applied to examine other types of composites. For instance, the CC has been utilized to study 3D transverse cracking and debonding in polymer matrix and glass fiber plain weave composites [29, 30], as well as 2D damage initiation and propagation in a ceramic matrix woven composite [31]. Furthermore, the failure mechanisms at the microscopic scale have been explored, including the debonding of a particle [32, 33] and the fiber-matrix interface [34–38] as well as the influence of the distance and angle between two neighbor fibers on interface debonding initiation [39].

A main difficulty in applying the CC in a 3D problem is determining the shape of the potential crack surface within a 3D geometry. A first way to implement the CC in 3D consists in assuming a crack path and applying stress and energy criteria corresponding to increasingly large cracks following this path. This strategy was adopted to study transverse cracking in laminates based on rectangular crack shapes [24, 26, 40] as well as partially elliptical crack shapes to simulate crack initiation at a V-notch [41–43], tunneling crack in layered ceramics [44] or free edge delamination in angle ply laminates [45]. Parameterized crack shapes may not be the optimal crack shapes, i.e. the ones for which the initiation loading is the minimum. A tentative to get crack shapes closer to the optimal ones consists in defining the crack fronts based on the stress isocontours [46–48]. This approach yields crack shapes that are similar to those observed experimentally in some configurations [49, 50] and enables the possible initiation crack shapes to be described by a single parameter, i.e. the crack surface or equivalently, the associated stress isocontour level. It results in an efficient way to avoid testing all possible crack shapes and was implemented for various 3D configurations [51–54].

It has been shown here that the CC is a pertinent tool to be used during an optimization process taking into account the recommendation of the Military Handbook. Current manufacturing methods, such as automated fiber placement, due to their precision and the intricate deposition paths they facilitate, should pave the way for increasingly complex and optimized stacking sequence such as Bouligand laminates which exhibits lower damage than classical laminates [55]. However, due to the lack of data, the absence of design rules, and conservatism arising from traditional practices, many industries continue to rely solely on 0°, ±45°, and 90° plies. Indeed, the use of varied ply orientations can lead to more complex damage scenarios. Literature has shown that the stacking sequence can significantly affect both the onset and progression of damage, not only in the initially failed ply but also in adjacent plies [56, 57].

The objective of this work is to study crack initiation in θ-plies that are adjacent to a 90° ply in a composite laminate. Experiments carried out on laminates having both 90° and θ°-plies are first presented in Section 2. The aim of this section is to highlight the effect of different parameters (ply thicknesses, angle differences between 90° and θ°-plies on the threshold for the initiation of transverse cracks in each ply. The finite element model and the CC procedure are described in Section 3. Section 4 focuses on evaluating different damage mechanisms such as crack initiation in (i) 90° ply and (ii) θ-ply, as well as (iii) debonding (delamination) between 90° ply and θ-ply. A qualitative comparison to the damage mechanisms observed experimentally is finally provided.

2. Experiments

The laminates under investigation were manufactured from Hexcel ply prepreg with AS4 carbon fibers and 8552 matrix. The panels were fabricated using a press machine, following the pressure and temperature cycles recommended by the prepreg manufacturer. One ply thickness corresponds to $t_{\text{ply}} = 150$ µm. The aim of this section is to highlight the influence of various parameters on the strain threshold for transverse crack initiation in the plies. To achieve this, different layups and stacking sequences were investigated:

- $[30_2/90_2/-30_2/0]_s$ is the base line (see Figure 1). It is expected that the 90° plies will crack first, and that any transverse cracking in the 30° plies will occur only at a loading level approaching failure.
- The $[70_2/90_2/-70_2/0]_s$ layup is designed to investigate whether a crack initiated in a misaligned ply can reinitiate cracking in an adjacent ply. It is important to note that, in this case, the doubled-thickness −70° plies are embedded within the laminate, while the other doubled-thickness 70° plies are located on the outer surface. As shown in [58], the position of the ply within the laminate (whether embedded or on the outer surface) influences the in-situ strength.
- The $[70_2/0/90_2/0/-70_2]_s$ layup is used to investigate the confinement effect of a highly oriented ply (0° in this case) on crack reinitiation. In this case, the outer plies are doubled-thickness 70° plies, while the ply located in the laminate's symmetry plane is a quadrupled-thickness −70° ply.
- The $[70_4/90_4/-70_4/0]_s$ layup is used to study the effect of ply thickness on crack reinitiation.

The specimen surfaces, where cracks are observed, are polished using silicon carbide paper with grit sizes ranging from P80 to P4000. A thin layer of white paint is then applied to these surfaces using a Posc® marker pen (Uni Mitsubishi Pencil). This thin layer of white paint facilitates crack detection, as cracks appear black against the white background. During the test, the gauge length is monitored using a high-resolution camera (4504 × 4504 pixels, with a 50 mm lens). Particular attention has been paid to the lighting to ensure that the light exposure is as even
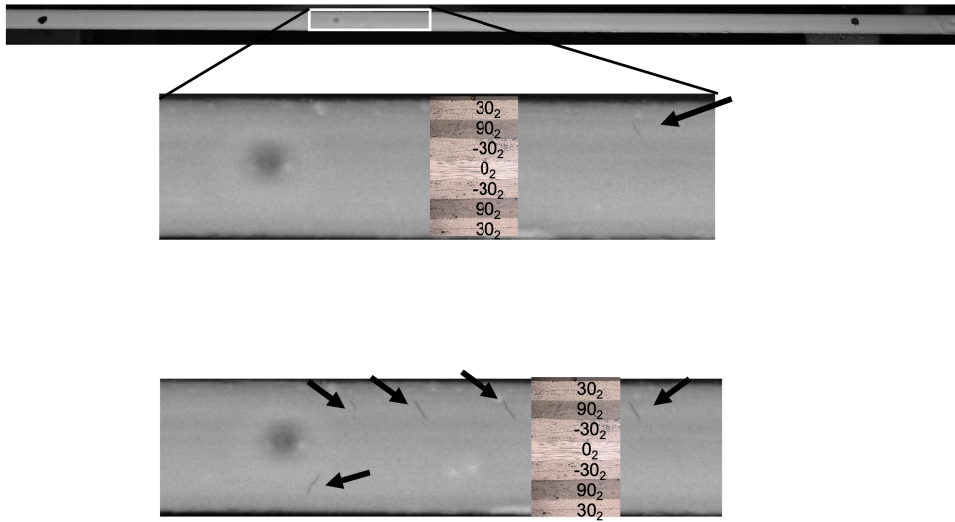
Figure 1. Location of the first cracks in the $[30_2/90_2/-30_2/0]_s$ laminate under two levels of external loading. A representative cross-sectional image has been included to indicate the ply locations (not visible due to the white paint layer). The arrows highlight the crack locations in the 90° plies.
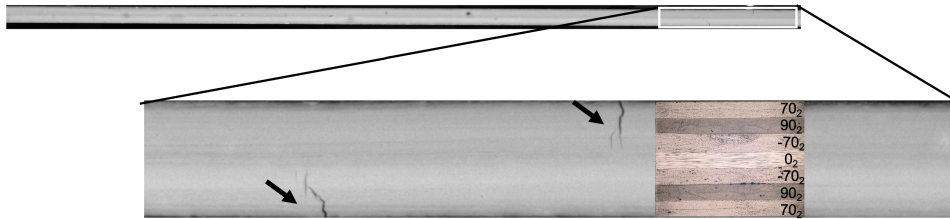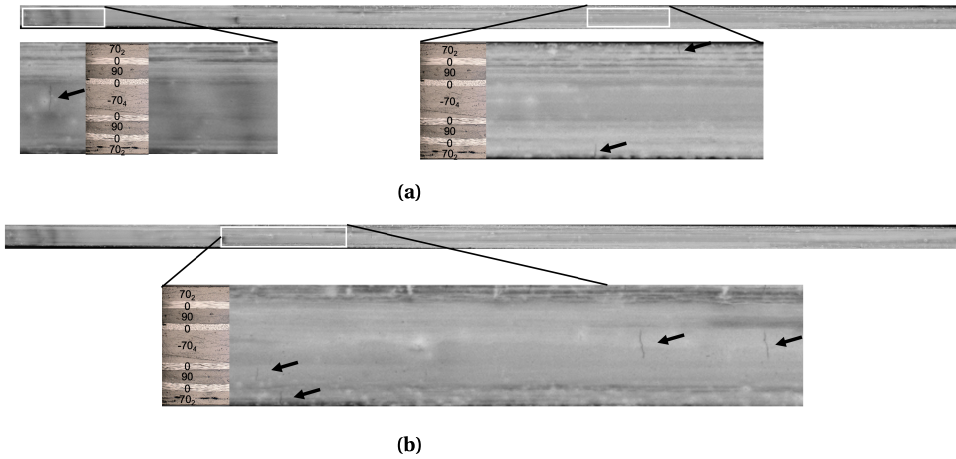

Figure 2. Location of the first cracks in the $[70_2/90_2/-70_2/0]_s$ laminate. A representative cross-sectional image has been included to indicate the ply locations (not visible due to the white paint layer). The arrows highlight the crack locations in the plies.

as possible and remains constant throughout the test. The aim is to detect the crack initiation in each ply and its location. The evolution in the number of cracks during testing falls outside the scope of this study.

The results obtained in the base line are shown in Figure 1. The first crack is initiated in the 90_2 plies. The number of cracks in these plies increases until final failure occurs, driven by delamination (between the 90° plies and the ±30° plies) and fiber failure in the 0° plies.

If the ±30 plies are replaced by ±70 plies, ($[70_2/90_2/-70_2/0]_s$) the scenario changes significantly. The initial failures occur simultaneously in all off-axis plies, namely the outer 70° plies, the 90° plies, and the −70° plies (see Figure 2). It is important to note that cracks in adjacent plies are interconnected, suggesting that a crack initiated in one ply may lead to the initiation of a crack in an adjacent ply.

When the 0° plies are placed between the 90° plies and the ±70° plies (as in the $[70_2/0/90_2/0/-70_2]_s$ laminate), transverse cracks initiate in the ±70° plies (Figure 3a). The locations of cracks in the outer doubled-thickness 70° plies differ significantly from those in the quadrupled-thickness −70° ply. The first cracks in the 90° plies initiate at a slightly higher

(a)

(b)

Figure 3. Location of the cracks in the $[70_2/0/90_2/0/-70_2]_s$ laminate. (a) Initial cracks in the $\pm 70°$ plies and (b) first crack in the 90° ply, occurring at a higher load. A representative cross-sectional image indicates ply locations (not visible due to the white paint layer). The arrows highlight crack locations within the plies.

applied load (see Figure 3b). The crack locations in the plies appear random, with no observable connection between cracks in different plies.

To conclude this experimental section, it is important to note that, on the one hand, when the angular difference between two adjacent plies is large, a matrix crack in the more misaligned ply does not initiate a crack in the adjacent ply, as in the baseline case $[30_2/90_2/-30_2/0]_s$. On the other hand, when the mismatch angle between two adjacent plies is small, a crack in one ply can initiate interconnected cracks in the adjacent plies, as observed in the $[70_n/90_n/-70_n/0]_s$ laminate with $n = 2$ or 4, a phenomenon not predicted by classical design approaches. A single ply with a large mismatch angle (in this case, the 0° ply between the $\pm 70°$ and 90° plies) could prevent this phenomenon. Another notable result concerns the effect of ply thickness: in the $[70_2/0/90_2/0/-70_2]_s$ laminate, the first matrix cracks appear in the outer doubled-thickness 70° plies and the quadrupled-thickness $-70°$ ply, rather than in the doubled-thickness 90° ply, which would be expected to fail first according to a simple failure criterion. The various observed mechanisms will be examined in the following sections using the CC.

3. Fracture modeling and simulation

3.1. *The coupled criterion*

The CC states that crack initiation occurs if the two following conditions are met:

- The incremental energy release rate ($\mathcal{G}_{inc}$), i.e. the ratio between the elastic strain energy release ($-\Delta W_{el}(S) = W_{el}(0) - W_{el}(S)$) due to the initiation of a crack and its surface (S) must be larger than the material critical energy release rate $\mathcal{G}_c$: $\mathcal{G}_{inc} \geq \mathcal{G}_c$
- The stress over the whole crack path prior to initiation must be sufficiently large. In homogeneous isotropic materials, it reverts to comparing the opening stress to the tensile strength. However, in anisotropic materials such as composite laminates, or for interfaces subjected to mixed mode loadings, a criterion combining the opening (σ_{nn}) and shear (σ_{nt}) stress components and the corresponding strengths can be used. For a lamina under tensile loading, the transverse crack initiation criterion can be described

using a Hashin-based failure criterion: $f(\underline{\sigma}, Y_t, S_c) = \sqrt{(\sigma_{nn}/Y_t)^2 + (\sigma_{nt}/S_c)^2} \geq 1$ where σ_{nn} and σ_{nt} represent the transverse and shear components of the stress tensor in the ply coordinate system. The parameters Y_t and S_c denote the transverse tensile strength and the shear strength, respectively.

Under linear elasticity and small deformation assumptions, the stress components are proportional to the applied strain (denoted ε_0) and the energy is proportional to the square applied strain. These conditions write:

$$\begin{cases} \sigma_{eq} = \sqrt{(\sigma_{nn})^2 + \left(\dfrac{\sigma_{nt}}{\alpha}\right)^2} = \xi(S)\varepsilon_0 \geq \sigma_c \\ \mathcal{G}_{inc} = A(S)\varepsilon_0^2 \geqslant \mathcal{G}_c \end{cases} \tag{1}$$

where $\alpha = S_c/Y_t$, $\sigma_c = Y_t$ and ξ and A are functions depending on the geometry and material properties. Note that in the following, we study configurations in which the stress field in the ply is either uniform (Sections 4.1 and 4.2) or present a gradient (Section 4.4) The strain that must be prescribed in order to fulfill either the stress or the energy conditions can be calculated from Equation (1):

$$\begin{cases} \varepsilon_0^{stress}(S) = \dfrac{\sigma_c}{\xi(S)} \\ \varepsilon_0^{energy}(S) = \sqrt{\dfrac{\mathcal{G}_c}{A(S)}} \end{cases} \tag{2}$$

For a given crack surface S, the strain that must be prescribed in order to fulfill Equation (1) is the maximum between $\varepsilon_0^{stress}(S)$ and $\varepsilon_0^{energy}(S)$. The applied strain at initiation ε_c is thus determined for the crack surface S_c that minimizes the applied strain:

$$\begin{cases} \varepsilon_c = \min_S(\max(\varepsilon_0^{stress}(S), \varepsilon_0^{energy}(S))) \\ S_c = \arg\min_S(\max(\varepsilon_0^{stress}(S), \varepsilon_0^{energy}(S))) \end{cases} \tag{3}$$

3.2. *Finite element model of laminates*

The configuration under investigation is $[0_n/-\theta_n/\theta_n/90_n]_s$, except in Section 4.4 where $[-\theta_n/\theta_n/0_n/90_n]_s$ stacking is studied to highlight the influence of the presence of a 0° ply in between 90° and θ° plies. Even if the stacking sequences studied numerically slightly differ from the tested ones, they allow assessing the different damage mechanisms observed experimentally. The FE models presented in the following are set-up using Abaqus™ Standard. Due to the loading and geometry symmetry, only half the laminate thickness is modeled. The thickness of n plies is denoted t, so that $t = nt_{ply}$. It means that when studying θ-ply crack initiation, one crack is present in the n θ-plies (thickness t) in the FE model, which actually represents the simultaneous cracking of the two sets of n θ-plies by symmetry. In addition, when studying 90° ply crack initiation, one crack is present in the n 90° plies (thickness t) in the FE model, which actually represents cracking in a set of $2n$ 90° consecutive plies by symmetry since the 90° ply lies on the symmetry plane. Crack opening for all the studied mechanisms (transverse cracking in a 90° ply, in θ-ply or debonding) are simulated by doubling the nodes along the corresponding surface. The ply angle refers to the angle formed between the loading direction and the fiber orientation within the ply. Since crack paths are oriented by the microstructure, they are likely to follow the fiber direction therefore cracks in θ-ply form a θ angle with respect to the loading direction. The material orientation of each ply is assigned and the same ply properties are defined in the corresponding ply local axis system. The transversely isotropic ply properties are $E_L = 127$ GPa, $E_T = 9.2$ GPa, $\nu_{LT} = 0.302$, $\nu_{TT} = 0.4$, $G_{LT} = 4.8$ GPa [27, 59], where the index L denotes the longitudinal fiber direction and T the direction perpendicular to the fibers in the ply plane. The ply
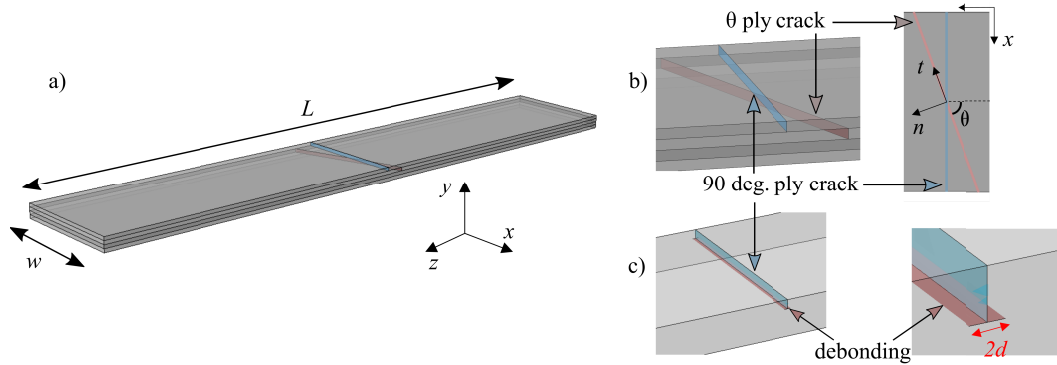
Figure 4. Geometry and dimensions of (a) the tested specimens and of two possible mechanisms occurring after transverse crack initiation in a 90° ply: (b) cracking in θ-ply or (c) debonding between 90° and θ-ply. The loading direction is along $\vec{z}$.

transverse tensile and shear strengths are respectively $Y_t = 63.9$ MPa and $S_c = 91$ MPa, the ply critical energy release rate is 248 J/m^2 [27], which corresponds to transverse crack propagation under opening mode. Boundary conditions are set-up as imposed displacement on the specimen faces along the tensile loading direction (z in the Figure 4). Due to the symmetry of the laminate, only half of the layup is modeled, with symmetric boundary conditions applied along the plane $(O\vec{x}, \vec{z})$. The meshes are made of 10-nodes quadratic tetrahedrons, the mesh size being refined in the vicinity of the crack or debonding locations, resulting in meshes with around 250,000 nodes. The mesh size is chosen so that a finer mesh provides a similar initiation loading.

3.3. *Transverse crack initiation*

The main difference between 2D and 3D simulation of transverse crack initiation in laminates arises from the fact that the stress field is not perfectly homogeneous in the whole ply but only in the ply center, the stress increasing closer to the ply free edge. Nevertheless, it was shown by Garcia et al. [24] that the 2D or the 3D applications of the CC for transverse crack initiation leads to similar initiation strain, especially for plies thinner than the Irwin's length $\ell_{\mathrm{mat}} = E_T \mathcal{G}_c / \sigma_c^2$. The differences slightly increase with increasing ply thickness, they however remain smaller than 10%. Therefore, in this case it is possible to simplify the 3D application of the CC for transverse crack initiation by neglecting the stress variation near the 90° ply free edge and considering a constant homogeneous stress within the ply. Under this assumption, Equation (3) reduces to:

$$\varepsilon_c = \max(\varepsilon_0^{\mathrm{stress}}(S_{90}), \varepsilon_0^{\mathrm{energy}}(S_{90})) = \max\left(\frac{\sigma_c}{\xi_{90}(S_{90})}, \sqrt{\frac{\mathcal{G}_c}{A_{90}(S_{90})}} \right) \tag{4}$$

where $S_{90} = w t_{90}$ is the surface of the crack crossing the whole ply. The functions $\xi_{90}(S_{90})$ and $A_{90}(S_{90})$ (corresponding to the functions ξ and A involved in Equation (2) in the case of transverse cracking) are computed from two FE calculations, one before crack opening that enables the calculation of the stress condition (and thus $\xi_{90}(S_{90})$) and the elastic strain energy before initiation, then crack surface nodes are unbuttoned to calculate the elastic strain energy release due to crack initiation and to deduce $A_{90}(S_{90})$. Transverse crack initiation loading is finally calculated from Equation (4).

3.4. *Debonding*

A possible damage mechanism occurring after transverse crack initiation is debonding between the 90° and θ-ply. This occurs because of the presence of a transverse crack in the 90° ply induces a stress singularity at the interface between both plies. It can be noted that under in-plane tensile loading, the interface is parallel to the loading direction thus debonding is not likely to occur without the presence of a crack in a surrounding ply. For the sake of simplicity, we assume that symmetric debonding occurs ahead of the transverse crack and along the whole ply width. This assumption allows us to describe the inter-ply debonding by only one parameter, namely the debonding length $2d$, the corresponding debonding surface being calculated as $S_d = 2dw$, where w is the sample width. Thus, the CC for debonding length calculation can be applied following the reasoning described in Section 3.1. We make the hypothesis that the same material strength and fracture toughness as for transverse crack can be used in the case of debonding. This is justified by the fact that both mechanisms involve matrix cracking and fibre-matrix debonding at the microscopic scale. The function ξ_d and A_d (corresponding to the functions ξ and A involved in Equation (2) in the case of inter-ply debonding) are computed based on FE calculations for several debonding lengths. Since debonding occurs after transverse crack initiation, two possible cases may arise:

- If both the stress and the energy criteria are fulfilled for the loading corresponding to 90° ply transverse crack initiation, thus debonding is likely to occur instantaneously after transverse crack initiation.
- Otherwise, no debonding is observed when the transverse crack initiates so that the loading must be increased in order to initiate a debonding ahead of the transverse crack, the imposed debonding initiation strain can be calculated from Equation (3).

3.5. *Re-initiation in θ-ply*

Another possible damage mechanism occurring after transverse crack initiation is cracking in the θ-ply (Figure 2). In next section we study different scenarii, namely crack initiation in θ-ply alone, simultaneous crack initiation in 90° and θ-ply, or crack initiation in 90° followed by crack re-initiation mechanism in θ ply. For crack initiation in θ-ply alone, the exact same approach as for 90° ply crack initiation presented in Section 3.3 is adopted. For simultaneous crack initiation in 90° and θ-ply, a similar formulation as in Section 3.3 is adopted, except that the elastic strain energy release is calculated for a total crack surface which is the sum of both 90° and θ ply cracks.

The main difference in the CC implementation compared to the two previous scenarii arises for crack re-initiation in θ-ply. This is mainly due to the fact that the presence of a transverse crack in the 90° ply induces a stress singularity at the crack tip, i.e. at the interface between 90° and θ-ply, which results in a heterogeneous stress field in θ-ply. Therefore, the CC can be applied to assess crack re-initiation in θ-ply after the nucleation of a first transverse crack in the 90° ply. The stress heterogeneity in the θ-ply prevents us to adopt a simplified application of the CC and 3D crack initiation has to be studied. The critical step in the 3D CC application concerns the definition of the possible initiation crack shapes. We follow the approach proposed in [47–50, 52] to define the possible crack shapes based on the stress criterion isocontours (Figure 5). The main interest of this method is the definition of a unique relation between the stress level and the crack surface. Besides, for a given crack size, the stress criterion is strictly fulfilled since the crack shape is defined from the stress criterion isocontour. The corresponding crack surface is calculated based on the face area of the FE mesh elements attached to the crack. For a given configuration including a θ-ply, the functions ξ_θ and A_θ (corresponding to the functions ξ and A involved in Equation (2) in the case of crack re-initiation in θ-ply after a first transverse crack initiation in the
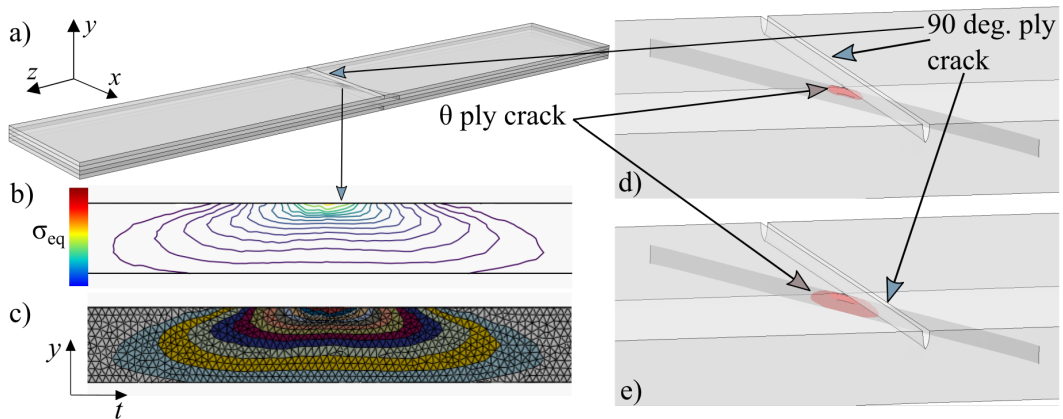
Figure 5. (a) Geometry including both 90° and θ-ply cracks. (b) Stress criterion isovalues in θ-ply after 90° ply crack initiation and (c) corresponding mesh including the stress criterion isocontour based possible crack shapes, (d)–(e) crack visualization in θ-ply.

90° ply) are computed by successively unbuttoning the crack nodes corresponding to decreasing stress isovalues or equivalently increasing crack surfaces. The re-initiation crack surface and imposed strain are finally determined by solving Equation (3). In the sequel, the numerical results corresponding to the different damage mechanisms are presented.

4. Results

We recall that the configuration under investigation is $[0_n/-\theta_n/\theta_n/90_n]_s$, except in Section 4.4 where $[-\theta_n/\theta_n/0_n/90_n]_s$ stacking is studied to highlight the influence of the presence of a 0° ply in between 90° and θ° plies.

4.1. *Crack initiation in 90° or θ° ply*

We first study transverse crack initiation in 90° or θ° ply. The CC enables the calculation of the strain that must be imposed in order to fulfill the stress criterion, the energy criterion, or both (Figure 6a). Crack initiation in a thick enough ($t > 0.6$ mm) 90° ply is controlled by the stress criterion. Indeed, a thick ply stores a sufficient amount of elastic energy that could be used to form a crack for imposed strain smaller than the imposed strain required to fulfill the stress criterion. Therefore, crack initiation occurs as soon as the stress criterion is fulfilled. This is not the case for a thin ply, for which not enough energy is available to create the crack when the stress criterion is fulfilled. Therefore, it results in a larger crack initiation imposed strain which corresponds to the strain required to fulfill the energy criterion. Figure 6b shows the 90° crack initiation imposed strain for several θ-ply configurations. The larger the disorientation between the 90° ply and the θ-ply, the larger the initiation imposed strain, even if the difference remains smaller than 10% for the studied configurations.

First crack initiation in a θ-ply is also studied and the variation of the initiation strain as a function the ply thickness is shown in Figure 6c. Whatever the ply orientation, the transition between energy-driven and stress-driven crack initiation is observed depending on the ply thickness. For a given ply thickness, the larger the ply misorientation, the larger the imposed strain at initiation. It can be concluded that if the θ-ply is not located at the specimen surface, 90° ply crack initiation is likely to be the first observed damage mechanism. In case the θ-ply
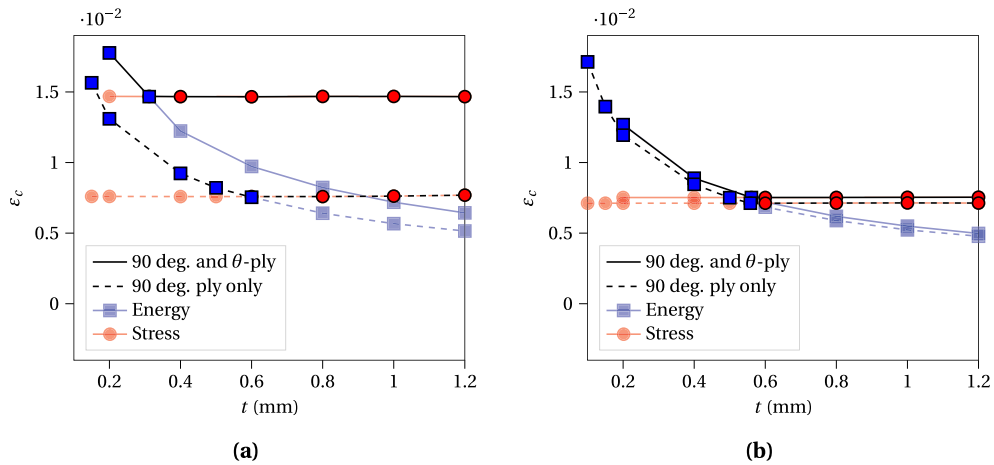
(a)

(b)

(c)
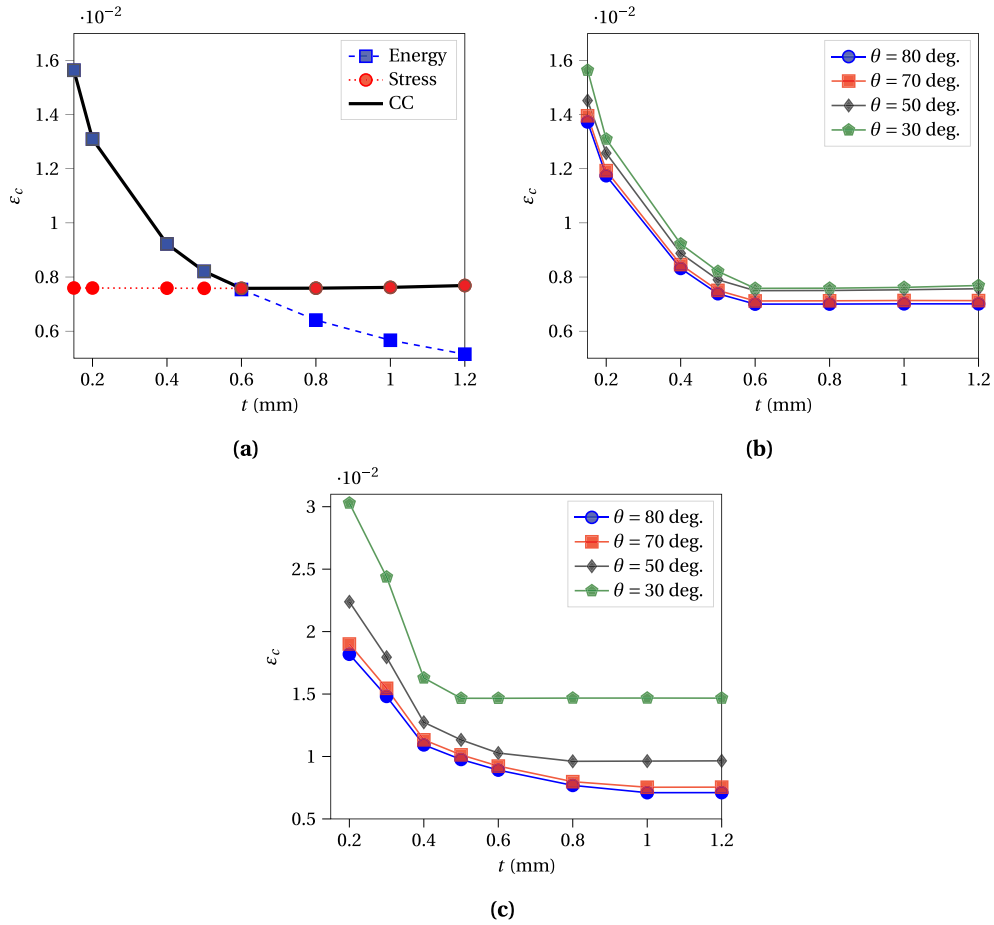
Figure 6. (a) Imposed strain to fulfill the stress (circles, dotted line), the energy (squares, dashed line) or both (solid line) criteria corresponding to 90° ply crack initiation as a function of the ply thickness for $\theta = 30$° ply orientation. (b) Imposed strain at 90° ply crack initiation as a function of the ply thickness for several θ-ply orientations of the adjacent ply. (c) Imposed strain at θ-ply crack initiation as a function of the ply thickness for several θ-ply orientations.

is located at the specimen surface, crack initiation in θ-ply may be more favorable than crack initiation in inner 90° depending on the ply thickness, as shown in Section 2.

For plies thicker than 0.6 mm, the stress criterion is fulfilled in the 90° ply at the crack initiation imposed strain, however it is not fulfilled in θ-ply because of the ply disorientation with respect to the loading direction. However, for plies thinner than 0.6 mm, crack initiation is driven by the energy criterion which means that the imposed strain may be large enough so that the stress criterion is fulfilled not only for the 90° ply but also for the θ-ply. Thus, another cracking mechanism could be envisioned, namely simultaneous crack initiation in both 90° ply and θ-ply.

4.2. *Simultaneous crack initiation in 90° ply and θ-ply*

The CC is applied in order to determine if simultaneous 90° ply and θ-ply crack initiation may occur instead of 90° ply crack initiation only for thin plies. Figure 7 shows the corresponding

Figure 7. Imposed strain to fulfill the stress (circles), the energy (squares) or both criteria corresponding to either 90° ply crack initiation (dashed line) or simultaneous 90° and θ-ply crack initiation (solid line) as a function of the ply thickness for (a) $\theta = 30°$ and (b) $\theta = 70°$.

imposed strain to fulfill the stress criterion, the energy criterion or both for configurations with 30° or 70° θ-ply.

The imposed strain required for crack initiation in thick plies is larger for simultaneous crack initiation than for 90° ply crack initiation only, thus resulting in a larger initiation imposed strain. Whatever the ply thickness and orientation, the imposed strain to fulfill the energy criterion is smaller for 90° ply crack initiation only than for simultaneous initiation. Therefore, simultaneous crack initiation in both plies is not likely to occur, the mechanism of crack re-initiation in θ-ply after first crack initiation in the 90° ply is therefore selected in the sequel.

4.3. *Debonding ahead of a 90°-ply crack*

Debonding at the interface between the 90° ply and the θ-ply is not likely to occur before any intra-ply cracking because the stress criterion is not fulfilled since the interface between both plies is parallel to the loading direction. However, the presence of a transverse crack in the 90° ply induces a stress singularity at the ply interface and thus enables a possible debonding between plies. The CC is applied in order to evaluate if debonding is likely to occur just after 90°, as depicted in Figure 4c. ply crack initiation or if a larger imposed strain is required. Two configurations arise leading either to a possible debonding or not. If the imposed strain is large enough so that there exists at least a debonding surface for which both criteria are fulfilled, a possible debonding may be observed as a consequence of transverse crack initiation and it occurs at the same imposed strain. Otherwise, if both criteria are not fulfilled for any debonding surface, debonding ahead of the transverse crack is not expected without imposed strain increase. The CC enables the calculation of the imposed strain required to initiate a debonding, its variation as a function of the ply thickness is shown in Figure 8 together with transverse crack initiation strain for $\theta = 50°$ and $\theta = 70°$ ply orientations.

For the studied configurations, debonding is not likely to occur just after transverse crack initiation except for the largest ply thicknesses θ-ply orientation close enough to 90°. Otherwise, the imposed strain must be increased in order to promote debonding ahead of the transverse crack.
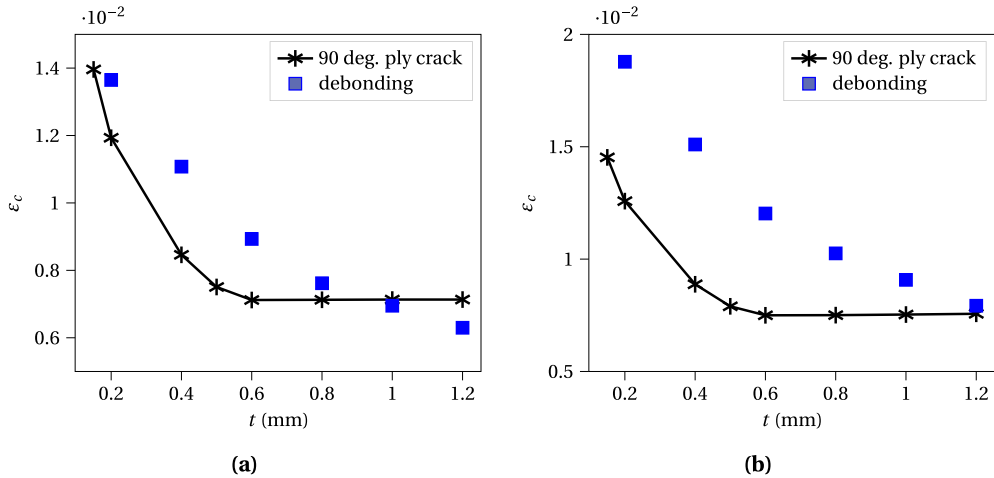
Figure 8. Imposed strain at debonding ahead of a transverse crack for (a) $\theta = 70°$ and $\theta = 50°$ ply orientations.
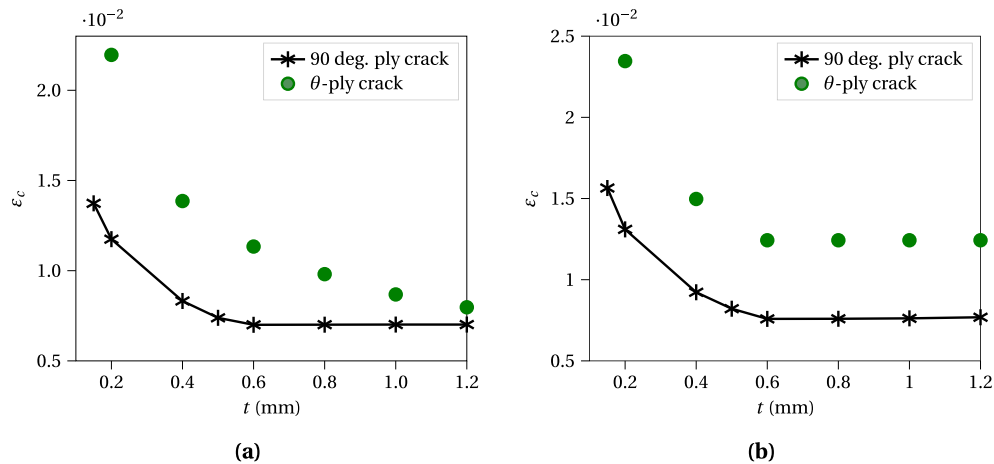
Figure 9. Imposed strain at crack re-initiation in θ-ply after the first crack initiation in the 90° ply as a function of the ply thickness for (a) $\theta = 80°$. (b) $\theta = 50°$ in case the θ-ply and the 90° ply are separated by a 0° ply.

4.4. θ-ply crack re-initiation

We first study the case for which the 90° ply and the θ-ply are separated by a 0° ply. The first damage mechanism is transverse crack initiation in the 90° ply. Similarly to previous analysis, simultaneous crack initiation in 90° ply and θ-ply is not likely to occur because it is energetically less favorable. Contrary to the configuration for which the 90° ply and the θ-ply are adjacent, crack initiation in the 90° ply does not induce any stress concentration in θ-ply. Therefore, crack re-initiation in the θ° ply may occur if both the stress and the energy criteria are fulfilled, i.e. for a larger imposed strain than the one corresponding to 90° ply crack initiation (Figure 9). If the 90° ply and the θ-ply are separated by a 0° ply, crack re-initiation is thus not likely to be observed immediately after the first crack initiation whatever the ply thickness or θ-ply orientation.
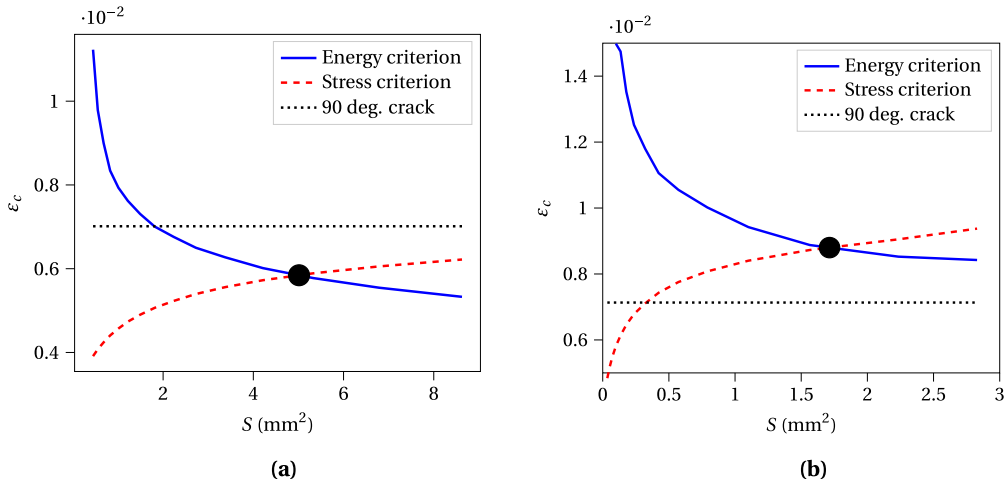
Figure 10. Imposed strain that must be prescribed in order to fulfill stress (dashed line) and energy (solid line) criteria and corresponding minimum imposed strain and crack surface for which both criteria are fulfilled (circle) for $t = 1$ mm ply thickness and (a) $\theta = 80°$ or (b) $\theta = 50°$.

We now study the configuration for which the 90° ply and the θ-ply are adjacent. A first crack initiation in the 90° ply induces a stress singularity at the crack tip located at the interface between both plies and thus a stress gradient in the θ-ply (Figure 5) which may promote θ-ply crack re-initiation. We use the term of re-initiation because we concluded previously that θ-ply crack initiation cannot occur simutaneously or before 90° ply crack initiation. Therefore, this mechanism is a consequence of a first crack initiation in the 90° ply which induces the stress singularity necessary to further enable a possible crack re-initiation. The stress and the energy criterion can be implemented in order to determine θ-ply re-initiation imposed strain as well as crack surface (Figure 10). If there exists a crack surface for which both criteria are fulfilled at the imposed strain corresponding to a first crack initiation in the 90° ply (Figure 10a), crack initiation immediately following 90° ply crack initiation is likely to occur. From an experimental point of view, it is difficult to detect both mechanisms separately since they are expected to occur sequentially in a short time interval. However, it is possible to observe whether a crack nucleated or not in θ-ply just after 90° crack initiation.

If fulfilling both criteria requires an imposed strain larger than the imposed strain at 90° ply crack initiation (Figure 10b), crack re-initiation in θ-ply is not likely to occur immediately after 90° ply initiation but requires an increase in the imposed strain. From an experimental point of view, it means that single crack initiation in the 90° ply is likely to be observed before θ-ply crack re-initiation for a larger imposed strain.

In both cases, it can be noted that the incremental energy release rate (and thus the differential energy release rate $\mathcal{G}$) is an increasing function of the crack surface. Therefore, as soon as crack initiation occurs, unstable crack propagation is likely to occur ($\mathcal{G} \geqslant \mathcal{G}_c$ and $d\mathcal{G}/dS \geqslant 0$). It means that without any increase in the imposed strain, the initiated crack will instantaneously grow through the entire ply. Therefore, the crack is expected to be observed experimentally on the specimen surface.

Figure 11 shows the imposed strain at θ-ply crack re-initiation as a function of the ply thickness and orientation. The imposed strain at crack re-initiation decreases with increasing ply thickness or decreasing ply disorientation (difference between 90° and the ply orientation θ).
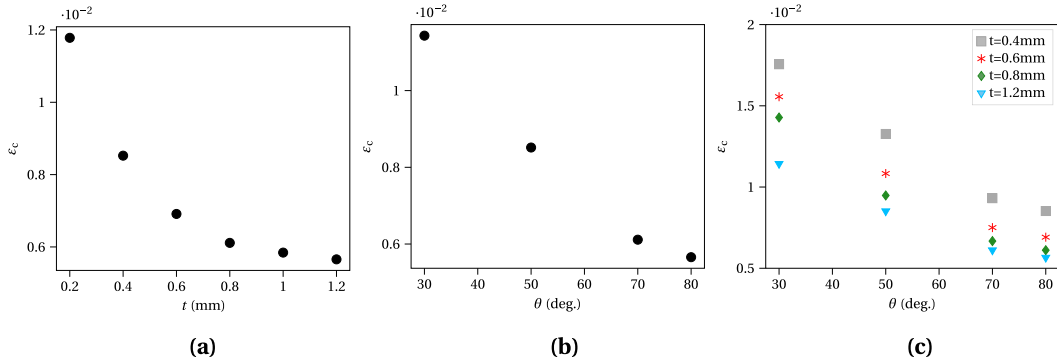
Figure 11. Imposed strain at θ-ply crack re-initiation as a function of (a) the ply thickness for $\theta = 70°$ and of the ply angle for (b) $t = 1.2$ mm or (c) for several ply thicknesses.
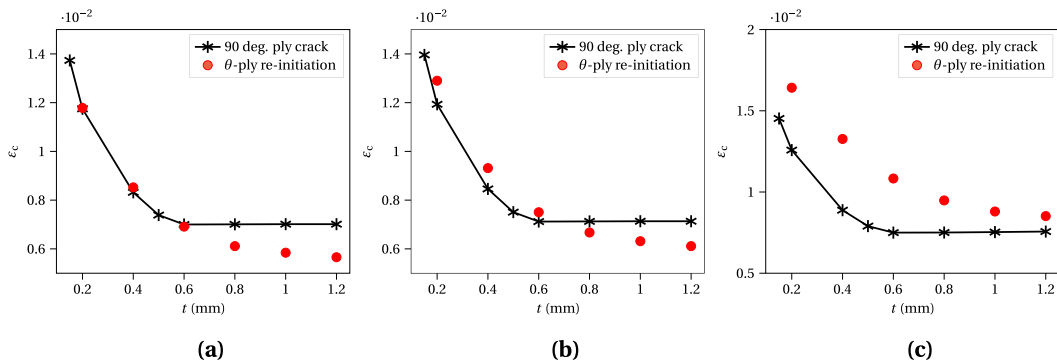
Figure 12. Imposed strain at θ-ply crack re-initiation as a function of the ply thickness compared to the imposed strain at 90° crack initiation for (a) $\theta = 80°$, (b) $\theta = 70°$, (c) $\theta = 50°$.
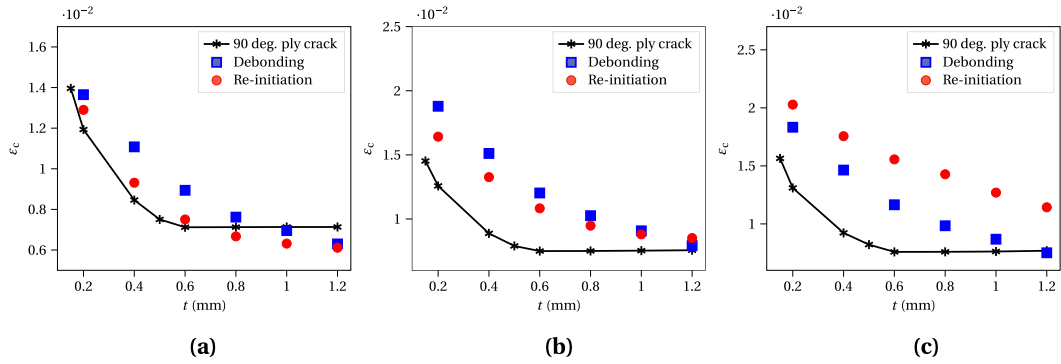
Figure 12 shows θ-ply crack re-initiation imposed strain as a function of the ply thickness compared to the imposed strain at 90° ply crack initiation for several ply orientations, resulting in different possible scenarii. If the ply orientation is close to 90° (Figure 12a), crack re-initiation is likely to occur whatever the ply thickness. We thus expect to observe experimentally cracks in both plies just after initiation. On the contrary, if the ply disorientation with respect to 90° is too large (Figure 12c), no crack re-initiation is expected to occur just after transverse crack initiation, it would require a larger imposed loading. For intermediate orientations (Figure 12b), crack re-initiation is expected to occur just after transverse crack initiation only for thick enough plies ($t > 0.6$ mm).

We finally compare the three damage mechanisms, namely transverse crack initiation, debonding and θ-ply crack re-initiation (Figure 13) for several ply orientation. For ply orientation close to 90° (Figure 13a) and thick enough plies ($t > 1$ mm), both debonding or crack re-initiation are likely to occur just after transverse crack initiation. For thin plies ($t < 6$ mm), the damage sequence that is likely to occur is the following order:

 (i) transverse crack initiation
 (ii) θ-ply crack re-initiation at a slightly larger imposed strain
 (iii) possible inter-ply debonding.

For intermediate ply thicknesses, crack re-initiation is likely to occur just after transverse crack initiation without any imposed strain increase, and debonding may occur for a larger imposed

Figure 13. Imposed strain at (i) 90° ply transverse cracking (solid line), (ii) inter-ply debonding (square symbols) or (iii) θ-ply crack re-initiation (disk symbols) as a function of the ply thickness t obtained for (a) $\theta = 70°$, (b) $\theta = 50°$, (c) $\theta = 30°$.

strain. For ply orientation different enough from 90° (Figure 13c), whatever the ply thickness, the most likely damage sequence is transverse crack initiation followed by debonding at a larger imposed strain. Crack re-initiation could possibly occur at a larger imposed strain. For intermediate ply orientation (Figure 13b), whatever the ply thickness, the most likely damage sequence is transverse crack initiation followed by crack re-initiation at a larger imposed strain. The observed change in the predicted sequence of damage mechanisms for different theta ply angles can be explained due to the critical strain for re-initiation changes a lot with θ ply misorientation, whereas the critical strain for debonding changes much less.

5. Discussions and conclusion

Composite materials offer significant potential for optimization in terms of the number of plies, ply orientations, and stacking sequences. However, the potential offered by new manufacturing techniques, such as automated fibre placement, is not being fully exploited due to the conservative practices currently in place. These practices are used to address the lack of predictive tools for mechanisms that may lead to domino cracking through the thickness of the laminate. In this article, we propose an approach based on the use of the coupled criterion, implemented using 3D finite element calculations.

To attain this objective, numerical simulations were conducted to investigate the damage mechanisms occurring in laminates with θ-plies adjacent to 90° plies. The results indicate that the damage sequence depends on the orientation mismatch between the 90° ply and the θ-ply. Several mechanisms can be identified. The deformation leading to the initiation of the first crack depends on both the ply thickness and the angle between the fiber orientation in the ply and the applied loading direction. For equivalent ply thicknesses, the greater the misorientation of the ply with respect to the loading axis, the smaller the deformation leading to the initiation of the first crack. However, this conclusion is called into question by the thickness of the plies. For instance, a thin ply oriented at 90° may undergo greater deformation before failure than a thicker, less misoriented ply. This conclusion is supported by experimental results. In the $[70_2/0/90_2/0/-70_2]_s$ laminate, the first cracks are initiated almost simultaneously in the doubled-thickness outer 70° ply and in the quadrupled-thickness inner $-70°$ ply.

This mechanism possibly enables two other mechanisms (that cannot occur without the presence of this first crack), namely either inter-ply debonding or crack re-initiation in adjacent θ-ply. These two mechanisms may possibly occur at the same imposed loading as the one

necessary for transverse crack initiation, if the ply is the θ-ply orientation close enough to 90° This conclusion is supported by experimental results. In the $[70_2/0/90_2/-70_2/0]_s$ laminate, the first cracks are initiated simultaneously in the $\pm70°$ and 90° plies. Moreover, all the cracks in the adjacent plies are continuous. Based on the results obtained for the previous laminate, it can be concluded that the crack first initiates in the outer 70° ply, leading to the failure of the adjacent plies.

If the angle offset between two adjacent plies is large, the most likely mechanism is debonding at the interface, initiated at the tip of the transverse crack. As observed experimentally in the $[70_2/0/90_2/0/-70_2]_s$ layup, a highly oriented ply (0° in this case), acts as a barrier, preventing crack re-initiation.

This study thus provides insight towards optimal, less empirical and less restrictive design of laminate stacking sequences. The results presented in this article were obtained using a thermoset matrix composite. Future work will focus on extending this study to thermoplastic matrix composites, which have much higher critical energy release rates. Moreover, for the $[30_2/90_2/-30_2/0]_s$ laminate, the cracks in the 90° ply appear to be slightly inclined, which motivates the investigation of the underlying phenomenon.

Declaration of interests

The authors do not work for, advise, own shares in, or receive funds from any organization that could benefit from this article, and have declared no affiliations other than their research organizations.

Dedication

The manuscript was written through contributions of all authors. All authors have given approval to the final version of the manuscript.

Acknowledgment

References

[1] MIL-HDBK-17-3F, *Composite Materials Handbook Volume 3. Polymer Matrix Composites Materials Usage, Design, and Analysis*, SAE International: USA, 2012.

[2] A. Parvizi, K. W. Garrett and J. E. Bailey, "Constrained cracking in glass fibre-reinforced epoxy cross-ply laminates", *J. Mater. Sci.* **13** (1978), pp. 195–201.

[3] M. R. Wisnom, B. Khan and S. R. Hallett, "Size effects in unnotched tensile strength of unidirectional and quasi-isotropic carbon/epoxy composites", *Compos. Struct.* **84** (2008), no. 1, pp. 21–28.

[4] M. R. Wisnom and S. R. Hallett, "The role of delamination in strength, failure mechanism and hole size effect in open hole tensile tests on quasi-isotropic laminates", *Compos. A: Appl. Sci. Manuf.* **40** (2009), no. 4, pp. 335–342.

[5] L. Lagunegrand, T. Lorriot, R. Harry, H. Wargnier and J. M. Quenisset, "Initiation of free-edge delamination in composite laminates", *Compos. Sci. Technol.* **66** (2006), no. 10, pp. 1315–1327.

[6] F. X. Irisarri, D. H. Bassir, N. Carrère and J. F. Maire, "Multiobjective stacking sequence optimization for laminated composite structures", *Compos. Sci. Technol.* **69** (2009), no. 7, pp. 983–990.

[7] K. S. Pister and S. B. Dong, "Elastic bending of layered plates", *J. Eng. Mech. Div., Proc. Am. Soc. Civil Eng.* **85** (1959), no. EM4, pp. 1–12.

[8] S. W. Tsai and H. T. Hahn, *Introduction to Composite Materials*, CRC Press: USA, 1980.

[9] F. Laurin, N. Carrere and J. F. Maire, "A multiscale progressive failure approach for composite laminates based on thermodynamical viscoelastic and damage models", *Compos. A: Appl. Sci. Manuf.* **38** (2007), no. 1, pp. 198–209.

[10] E. Iarve, M. Gurvich, D. Mollenhauer, C. Rose and C. Dávila, "Mesh-independent matrix cracking and delamination modeling in laminated composites", *Int. J. Numer. Meth. Eng.* **88** (2011), no. 8, pp. 749–773.

[11] S. R. Hallett, B. G. Green, W. G. Jiang and M. R. Wisnom, "An experimental and numerical investigation into the damage mechanisms in notched composites", *Compos. A: Appl. Sci. Manuf.* **40** (2009), no. 5, pp. 613–624.

[12] P. Journoud, C. Bouvet, B. Castanié, F. Laurin and L. Ratsifandrihana, "Experimental and numerical analysis of unfolding failure of L-shaped CFRP specimens", *Compos. Struct.* **232** (2020), article no. 111563.

[13] D. Leguillon, "A criterion for crack nucleation at a notch in homogeneous materials", *C. R. Acad. Sci. - Ser. IIB - Mech.* **329** (2001), no. 2, pp. 97–102.

[14] D. Leguillon, "Strength or toughness? A criterion for crack onset at a notch", *Eur. J. Mech. - A/Solids* **21** (2002), no. 1, pp. 61–72.

[15] E. Martin, D. Leguillon and N. Carrère, "Finite fracture mechanics: a useful tool to analyze cracking mechanisms in composite materials", in *Multi-scale Modelling of the Structural Integrity: 50 Years of Carbon Fiber Composite Materials* (P. W. R. Beaumont and C. Soutis, eds.), Springer: USA, 2016, pp. 529–548.

[16] P. P. Camanho, G. H. Ercin, G. Catalanotti, S. Mahdi and P. Linde, "A finite fracture mechanics model for the prediction of the open-hole strength of composite laminates", *Compos. A: Appl. Sci. Manuf.* **43** (2012), pp. 1219–1225.

[17] E. Martin, D. Leguillon and N. Carrère, "A coupled strength and toughness criterion for the prediction of the open hole tensile strength of a composite plate", *Int. J. Sol. Struct.* **49** (2012), no. 26, pp. 3915–3922.

[18] E. Martin, D. Leguillon and N. Carrère, "An extension of the point-stress criterion based on a coupled stress and energy fulfilment: application to the prediction of the open-hole tensile strength of a composite plate", in *Woodhead Publishing Series in Composites Science and Engineering, Structural Integrity and Durability of Advanced Composites*, Woodhead Publishing: UK, 2015, pp. 425–444.

[19] J. Felger, N. Stein and W. Becker, "Mixed-mode fracture in open-hole composite plates of finite-width: An asymptotic coupled stress and energy approach", *Int. J. Solids Struct.* **122–123** (2017), pp. 14–24.

[20] G. Catalanotti and P. P. Camanho, "A semi-analytical method to predict net-tension failure of mechanically fastened joints in composite laminates", *Compos. Sci. Technol.* **76** (2013), pp. 69–76.

[21] N. Carrere, N. Tual, T. Bonnemains, E. Lolive and P. Davies, "Modelling of the damage development in carbon/epoxy laminates subjected to combined seawater ageing and mechanical loading", *Proc. Inst. Mech. Eng. L: J. Mater.: Des. Appl.* **232** (2016), no. 9, pp. 761–768.

[22] M. Kashtalyan, I. G. García and V. Mantič, "Coupled stress and energy criterion for multiple matrix cracking in cross-ply composite laminates", *Int. J. Sol. Struct.* **139–140** (2018), pp. 189–199.

[23] A. Doitrand, G. Molnár, D. Leguillon, E. Martin and N. Carrère, "Dynamic crack initiation assessment with the coupled criterion", *Eur. J. Mech. - A/Solids* **93** (2022), article no. 104483.

[24] I. G. García, B. J. Carter, A. R. Ingraffea and V. Mantič, "A numerical study of transverse cracking in cross-ply laminates by 3D finite fracture mechanics", *Compos. B Eng.* **95** (2016), pp. 475–487.

[25] J. Vereecke, C. Bois, J. C. Wahl, T. Briand, L. Ballère and F. Lavelle, "Explicit modelling of meso-scale damage in laminated composites – Comparison between finite fracture mechanics and cohesive zone model", *Compos. Sci. Technol.* **253** (2024), article no. 110640.

[26] I. G. García, V. Mantič and A. Blázquez, "The effect of residual thermal stresses on transverse cracking in cross-ply laminates: an application of the coupled criterion of the finite fracture mechanics", *Int. J. Fract.* **211** (2018), pp. 61–74.

[27] I. G. García, J. Justo, A. Simon and V. Mantič, "Experimental study of the size effect on transverse cracking in cross-ply laminates and comparison with the main theoretical models", *Mech. Mater.* **128** (2019), pp. 24–37.

[28] E. Martin, D. Leguillon and N. Carrere, "A twofold strength and toughness criterion for the onset of free-edge shear delamination in angle-ply laminates", *Int. J. Solids Struct.* **47** (2010), no. 9, pp. 1297–1305.

[29] A. Doitrand, C. Fagiano, N. Carrère, V. Chiaruttini and M. Hirsekorn, "Damage onset modeling in woven composites based on a coupled stress and energy criterion", *Eng. Fract. Mech.* **169** (2017), pp. 189–200.

[30] A. Doitrand, C. Fagiano, F. Hild, V. Chiaruttini, A. Mavel and M. Hirsekorn, "Mesoscale analysis of damage growth in woven composites", *Compos. A: Appl. Sci. Manuf.* **96** (2017), pp. 77–88.

[31] J. Li, E. Martin, D. Leguillon and C. Dupin, "A finite fracture model for the analysis of multi-cracking in woven ceramic matrix composites", *Compos. B Eng.* **139** (2018), pp. 75–83.

[32] T. Gentieu, J. Jumel, A. Catapano and J. Broughton, "Size effect in particle debonding: comparisons between finite fracture mechanics and cohesive zone model", *J. Compos. Mater.* **53** (2018), no. 14, pp. 1941–1954.

[33] E. Martin, D. Leguillon, A. Catapano and N. Carrère, "Prediction of interfacial debonding between stiff spherical particles and a soft matrix with the coupled criterion", *Theor. Appl. Fract. Mech.* **109** (2020), article no. 102749.

[34] V. Mantič, "Interface crack onset at a circular cylindrical inclusion under a remote transverse tension. Application of a coupled stress and energy criterion", *Int. J. Sol. Struct.* **46** (2009), pp. 1287–1304.

[35] V. Mantič and I. G. García, "Crack onset and growth at the fibre-matrix interface under a remote biaxial transverse load. application of a coupled stress and energy criterion", *Int. J. Sol. Struct.* **49** (2012), pp. 2273–2290.

[36] I. G. García, M. Paggi and V. Mantič, "Fiber-size effects on the onset of fiber–matrix debonding under transverse tension: A comparison between cohesive zone and finite fracture mechanics models", *Eng. Fract. Mech.* **115** (2014), pp. 96–110.

[37] M. Muñoz-Reja, L. Távara, V. Mantič and P. Cornetti, "Crack onset and propagation at fibre–matrix elastic interfaces under biaxial loading using finite fracture mechanics", *Compos. A: Appl. Sci. Manuf.* **82** (2016), no. x, pp. 267–278.

[38] H. Girard, A. Doitrand, B. Koohbor, R. G. Rinaldi, N. Godin and J. Bikard, *Comparison between 2D and 3D fiber-matrix debonding simulation for inverse identification of interface fracture properties*, preprint, 2024. Online at https://hal.science/hal-04431332.

[39] H. Girard, A. Doitrand, B. Koohbor, R. G. Rinaldi, N. Godin, D. Long and J. Bikard, "Influence of nearby fiber on fiber–matrix debonding: Coupled Criterion prediction and debonding shape determination", *J. Mech. Phys. Solids* **183** (2024), article no. 105498.

[40] Z. Hamam, N. Godin, P. Reynaud, C. Fusco, N. Carrére and A. Doitrand, "Transverse cracking induced acoustic emission in carbon fiber-epoxy matrix composite laminates", *Materials* **15** (2022), article no. 394.

[41] B. Mittelman and Z. Yosibash, "Asymptotic analysis of the potential energy difference because of a crack at a V-notch edge in a 3D domain", *Eng. Fract. Mech.* **131** (2014), pp. 232–256.

[42] B. Mittelman and Z. Yosibash, "Energy release rate cannot predict crack initiation orientation in domains with a sharp V-notch under mode III loading", *Eng. Fract. Mech.* **141** (2015), pp. 230–241.

[43] Z. Yosibash and B. Mittelman, "A 3-D failure initiation criterion from a sharp V-notch edge in elastic brittle structures", *Eur. J. Mech. A/Sol.* **60** (2016), pp. 70–94.

[44] R. Papšík, O. Ševeček, A. K. Hofer, I. Kraleva, J. Kreith and R. Bermejo, "Prediction of edge and tunnelling crack formation in layered ceramics using a stress-energy fracture criterion", *J. Eur. Ceram. Soc.* **43** (2023), no. 7, pp. 2928–2934.

[45] M. Burhan, T. Scalici, Z. Ullah, Z. Kazanci and G. Catalanotti, "A three-dimensional Finite Fracture Mechanics model to predict free edge delamination in angle-ply laminates", *Eng. Fract. Mech.* **306** (2024), article no. 110156.

[46] D. Leguillon, "An attempt to extend the 2D coupled criterion for crack nucleation in brittle materials to the 3D case", *Theor. Appl. Fract. Mech.* **74** (2014), pp. 7–17.

[47] A. Doitrand and D. Leguillon, "3D application of the coupled criterion to crack initiation prediction in epoxy/aluminum specimens under four point bending", *Int. J. Sol. Struct.* **143** (2018), pp. 175–182.

[48] A. Doitrand and D. Leguillon, "Comparison between 2D and 3D applications of the coupled criterion to crack initiation prediction in scarf adhesive joints", *Int. J. Adhes. Adhes.* **85** (2018), pp. 69–76.

[49] A. Doitrand and D. Leguillon, "Numerical modeling of the nucleation of facets ahead of a primary crack under modeI+III", *Int. J. Fract.* **123** (2018), no. 1, pp. 37–50.

[50] A. Doitrand, R. Estevez and D. Leguillon, "Experimental characterization and numerical modeling of crack initiation in rhombus hole PMMA specimens under compression", *Eur. J. Mech. Sol.* **76** (2019), pp. 290–299.

[51] O. Sevecek, J. Hanak, Z. Majer, D. Drdlik, Z. Chlup and M. Kotoul, "Prediction of the ceramic foam structure failure using a detailed finite element model", *Key Eng. Mater.* **827** (2019), pp. 222–227.

[52] A. Doitrand, R. Henry, H. Saad, S. Deville and S. Meille, "Determination of interface fracture properties by micro- and macro-scale experiments in nacre-like alumina", *J. Mech. Phy. Sol.* **145** (2020), article no. 104143.

[53] A. Doitrand, R. Henry, I. Zacharie-Aubrun, J.-M. Gatt and S. Meille, "UO$_2$ micron scale specimen fracture: parameter identification and influence of porosities", *Theor. Appl. Fract. Mech.* **108** (2020), article no. 102665.

[54] N. Carrère, A. Doitrand, E. Martin and D. Leguillon, "Theoretical study based on 2D assumptions of the influence of small pores on crack initiation in adhesively bonded joints", *Int. J. Adhes. Adhes.* **111** (2021), article no. 102979.

[55] J. Körbelin, P. Goralski, B. Kötter, F. Bittner, H. F. Endres and B. Fiedler, "Damage tolerance and notch sensitivity of bio-inspired thin-ply Bouligand structures", *Compos. C: Open Access* **5** (2021), article no. 100146.

[56] T. Yokozeki, T. Aoki and T. Ishikawa, "Consecutive matrix cracking in contiguous plies of composite laminates", *Int. J. Solids Struct.* **42** (2005), pp. 2785–2802.

[57] S. Kobayashi, N. Takeda, S. Ogihara and A. Kobayashi, "Effects of stacking sequence on the transverse cracking in quasi-isotropic interleaved CFRP laminates", in *Proceedings of the 1999 International Conference on Composite Materials, Paris, France.*

[58] P. P. Camanho, C. G. Dávila, S. T. Pinho, L. Iannucci and P. Robinson, "Prediction of in situ strengths and matrix cracking in composites under transverse tension and in-plane shear", *Compos. A: Appl. Sci. Manuf.* **37** (2006), pp. 165–176.

[59] K. Marlett, *Hexcel 8852 AS4 unidirectional prepreg at 190 gsm and 35% RC qualification material property data report*, tech. rep., National Institute for Aviation Research. Wichita State University: Wichita, Kansas, 2010.